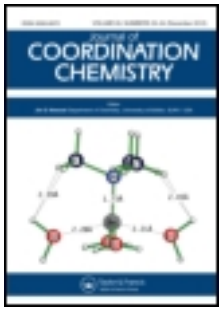

Journal of Coordination Chemistry
Publication details, including instructions for authors and subscription information:
http://www.tandfonline.com/loi/gcoo20

Synthesis, spectroscopic, and crystallographic characterizations of an antiferromagnetically coupled, oxobridged trinuclear manganese(IV) cluster $[Mn_3O_4(H_2O)_2(phen)_4](NO_3)_4 \cdot 3H_2O$ [phen=1,10-phenanthroline]

Bhaskar Biswas [a], Abhijit Pal [a], Partha Mitra [b], Floriana Tuna [c], Manabendra Mukherjee [d] & Rajarshi Ghosh [a]

[a] Department of Chemistry, The University of Burdwan, Burdwan 713 104, West Bengal, India

[b] Department of Inorganic Chemistry, Indian Association for the Cultivation of Science, Kolkata 700 032, West Bengal, India

[c] Department of Chemistry, The University of Manchester, Oxford Road, Manchester, M13 9PL, UK

[d] Surface Physics Division, Saha Institute of Nuclear Physics, Sector-1, Block-AF, Bidhannagar, Kolkata 700 064, West Bengal, India

Accepted author version posted online: 21 Sep 2012.Published online: 09 Oct 2012.

To cite this article: Bhaskar Biswas, Abhijit Pal, Partha Mitra, Floriana Tuna, Manabendra Mukherjee & Rajarshi Ghosh (2012) Synthesis, spectroscopic, and crystallographic characterizations of an antiferromagnetically coupled, oxobridged trinuclear manganese(IV) cluster $[Mn_3O_4(H_2O)_2(phen)_4](NO_3)_4 \cdot 3H_2O$ [phen=1,10-phenanthroline], Journal of Coordination Chemistry, 65:23, 4067-4076, DOI: 10.1080/00958972.2012.732694

To link to this article: http://dx.doi.org/10.1080/00958972.2012.732694

Journal of Coordination Chemistry
Vol. 65, No. 23, 10 December 2012, 4067–4076

Synthesis, spectroscopic, and crystallographic characterizations of an antiferromagnetically coupled, oxobridged trinuclear manganese(IV) cluster $[Mn_3O_4(H_2O)_2(phen)_4](NO_3)_4 \cdot 3H_2O$ [phen = 1,10-phenanthroline]

BHASKAR BISWAS†, ABHIJIT PAL†, PARTHA MITRA‡, FLORIANA TUNA§, MANABENDRA MUKHERJEE¶ and RAJARSHI GHOSH*†

†Department of Chemistry, The University of Burdwan, Burdwan 713 104, West Bengal, India
‡Department of Inorganic Chemistry, Indian Association for the Cultivation of Science, Kolkata 700 032, West Bengal, India
§Department of Chemistry, The University of Manchester, Oxford Road, Manchester, M13 9PL, UK
¶Surface Physics Division, Saha Institute of Nuclear Physics, Sector-1, Block-AF, Bidhannagar, Kolkata 700 064, West Bengal, India

(*Received 23 February 2012; in final form 27 August 2012*)

Design and synthesis of a triangular manganese compound, $[Mn_3O_4(H_2O)_2(phen)_4](NO_3)_4 \cdot 3H_2O$ (**1**) with mono-μ-oxo and di-μ-oxo, is described. The complex has been characterized by elemental analysis, spectroscopy, single crystal and powder diffraction measurements, thermogravimetric analysis, etc. Bond Valence Sum calculations and X-ray photoelectron spectroscopy reveal that each manganese at each vertex of the triangle is +IV oxidation state. Variable temperature magnetic measurements show strong antiferromagnetic coupling between metal ions with the following set of parameters: $g = 1.99$, $J_1 = -50.0\,cm^{-1}$, and $J_2 = -90.2\,cm^{-1}$ (where J_1 describes the interaction across the two mono-μ-oxo bridges and J_2 is the exchange coupling across the di-μ-oxo bridge). The compound breaks down in three steps when heated from room temperature to 900°C. The final ash of the compound is confirmed by infrared spectrum with standard MnO_2.

Keywords: Synthesis; Crystal structure; BVS calculation; XPS; Magnetism; Thermal property

1. Introduction

Design and synthesis of multinuclear transition metal coordination assemblies are of interest for diverse applications towards molecular magnetism [1], bio-mimicking chemistry [2], etc. Conventional magnets have collective behavior of the unpaired electron spins of millions of metal ions in a particle or bulk material. Single-molecule magnets (SMMs) [3], on the other hand, are transition-metal, homo-, or heterometallic

*Corresponding author. Email: chem_rghosh@buruniv.ac.in

ISSN 0095-8972 print/ISSN 1029-0389 online © 2012 Taylor & Francis
http://dx.doi.org/10.1080/00958972.2012.732694

clusters that individually exhibit properties of a magnet below a critical temperature (the blocking temperature, currently ~4 K). Their properties arise from the combination of a large spin value (S) in the ground state and significant magnetoanisotropy of the easy-axis type (manifested as a negative zero-field splitting parameter, D). Due to their small size, SMMs have also been shown to exhibit quantum tunneling of magnetization [4] and quantum phase interference [5]. Compared to other 3d metal ions, manganese clusters often have large spin ground states; this characteristic in combination with Jahn-Teller distortion of high-spin Mn^{III} in near-octahedral stereochemistry (the source of the single-ion anisotropy) make manganese clusters ideal candidates for SMM behavior [3d]. Manganese also plays a key role in different biological processes. In oxygen evolving complexes, it catalyzes the splitting of water [6]. Concerning manganese, two properties can be distinguished, Mn^{II} as a Lewis acid and in higher oxidation states (Mn^{III}, Mn^{IV}) as an oxidative catalyst [7]. Herein we describe synthesis, structural characterization, and magnetostructural correlations of an oxobridged trimetallic Mn(IV) triangle $[Mn_3O_4(H_2O)_2(phen)_4](NO_3)_4 \cdot 3H_2O$ (**1**).

2. Experimental

2.1. *Preparation of the complex*

(a) Chemicals, solvents and starting materials: High purity 1,10-phenanthroline (phen) (Fluka, Germany), ceric ammonium nitrate (Aldrich, UK), manganese(II) chloride tetrahydrate (E. Merck, India), and all reagents were purchased and used as received.
(b) Synthesis of **1**.

A 60–40 v/v AcOH-H_2O solution (10 cm^3) of 1,10-phenanthroline (0.198 g, 1 mmol) was added dropwise to a solution of $MnCl_2 \cdot 4H_2O$ (0.197 g, 1 mmol) in the same solvent (10 cm^3) and mixed slowly on a magnetic stirrer with slow stirring for 10 min. The solution turned pink. Then solid ammonium ceric nitrate (1.10 g, 2 mmol) was added portion-wise into the above solution and the pink solution turned to a dark brown clear solution. Stirring was continued for another 10 min. Lastly, the solution was filtered and the supernatant liquid was kept in air for slow evaporation. After a few days, the fine microcrystalline compound that separated was washed with toluene and dried *in vacuo* over silica gel indicator. The air-stable moisture-insensitive compound is soluble in polar solvents like methanol, ethanol, acetonitrile, and water. Yield: 0.152 g (77.1% based on metal salt). Anal Calcd for $C_{48}H_{42}N_{12}O_{21}Mn_3$ (**1**) (%): C, 44.87; H, 3.28; N, 13.05. Found (%): C, 44.84; H, 3.21; N, 13.12. IR (KBr pellet, cm^{-1}): 3418, 1604, 1587, 1384, 852. UV-Vis (λ, nm): 234, 269, 418, 488.

2.2. *Physical measurements*

Elemental analyses (carbon, hydrogen and nitrogen) were performed on a Perkin Elmer 2400 CHNS/O elemental analyzer. IR spectrum was recorded (KBr discs, 4000–300 cm^{-1}) using a Perkin Elmer RX1 FTIR spectrometer. Ground state absorption was measured with a JASCO V-530 UV-Vis spectrophotometer.

Solid-state, variable-temperature (2.0–300 K) dc magnetic susceptibility data using a 1000 G (0.1 T) magnetic field were collected on polycrystalline samples with a Quantum Design MPMS-XL SQUID magnetometer equipped with a 7 T magnet. Isothermal magnetization *versus* field studies was performed at 2 and 4 K by varying the magnetic field between 0 and 7 T. All data were corrected for diamagnetism by using Pascal constants and for the diamagnetic contribution of the sample holder by measurement.

2.3. *Powder X-ray diffraction study*

The X-ray diffraction pattern was registered with a Bruker D8 AXS Powder X-ray diffractometer under continuous scanning mode in the 2θ range 10°–80° ($\lambda = 1.5405$ Å) and step size $\Delta 2\theta = 0.0195°$ working with Cu-Kα radiation.

2.4. *Single crystal X-ray diffraction study*

Crystal diffraction data were measured using a Bruker SMART APEX CCD diffractometer. The data were collected with graphite monochromated Mo-Kα radiation ($\lambda = 0.71073$ Å) at 200 K. The structure was solved by direct methods and refined by full-matrix least-squares using the SHELXL-97 software package [8, 9]. The crystallographic data are summarized in table 1.

Table 1. Crystallographic data of **1**.

Crystal parameters	**1**
Empirical formula	$C_{48}H_{42}N_{12}O_{21}Mn_3$
Formula weight	1279.69
Temperature (K)	296(2)
Wavelength (Å)	0.71073
Crystal system	Triclinic
Space group	*P*1 (No. 2)
Unit cell dimensions (Å, °)	
a	10.661(2)
b	12.448(2)
c	20.354(4)
α	78.732(5)
β	83.015(5)
γ	81.832(6)
Volume (Å^3), *Z*	2609.9(8), 2
Calculated density (Mg m^{-3})	1.628
Absorption coefficient (mm^{-1})	0.809
F(000)	1298
θ range for data collection (°)	2.23–28.30
Index ranges	$-9 \le h \le 9$, $-11 \le k \le 11$, $-17 \le l \le 17$
Reflections collected	14,919
Independent reflection	3803 [*R*(int) = 0.054]
R indices (all data)	$R_1 = 0.0459$, $wR_2 = 0.1435$
Largest difference peak and hole (e Å^{-3})	0.58 and −0.31

2.5. *Magnetic property*

The magnetic properties of **1** were studied by a SQUID magnetometer in the 1.8–300 K temperature range in an applied magnetic field of 0.1 T.

2.6. *X-ray photoelectron spectroscopy*

XPS core-level spectra were taken with an Omicron Multiprobe (Omicron NanoTechnology GmbH., UK) spectrometer fitted with an EA125 hemispherical analyzer. A monochromated Al Kα X-ray source operated at 150 W was used for the experiments. The analyzer pass energy was kept fixed at 40 eV for all the scans. As the samples are insulating, a low energy electron gun (SL1000, Omicron) with a large spot size was used to neutralize the samples. The potential of the electron gun was kept fixed at −3 eV for all the samples with respect to the ground. The binding energy of the peaks was corrected by shifting the peak positions by an amount equal to that required to shift the main peak of the corresponding C1s spectrum to 285.0 eV.

2.7. *Thermal study*

The thermal behavior of **1** was followed up to 900°C in a static nitrogen atmosphere with a heating rate of 10°C per minute. $[Mn_3(phen)_4(O)_4(OH_2)_2](NO)_4 \cdot 3H_2O$ (**1**) decomposes in three steps.

3. Results and discussion

3.1. *Synthesis and formulation*

The oxobridged trinuclear manganese complex was synthesized from manganese(II) chloride, ammonium ceric nitrate and 1,10-phenanthroline (phen) using 1 : 2 : 1 molar ratio in AcOH–H_2O mixture at room temperature. The compound was characterized using elemental analysis and spectroscopic tools. The IR spectrum shows an asymmetric nitrate $\nu(NO_3)$ and bridged bent oxo ν(Mn–O–) stretches [10] centered at 1384 and 852 cm^{-1}, respectively. Peaks at 1604 and 1587 cm^{-1} are for the imine bonds.

3.2. *Powder X-ray pattern*

In Supplementary material, the powder X-ray diffraction (PXRD) pattern of $[Mn_3O_4(H_2O)_2(phen)_4](NO_3)_4 \cdot 3H_2O$ is provided. The peaks were indexed with the triclinic structure with $P\bar{1}$ space group. The powder pattern was analyzed using the FULLPROF refinement program [11] and the corresponding fits are also shown in Supplementary Material. The extracted cell parameters are $a = 10.6609$ Å, $b = 12.4470$ Å, $c = 20.3539$ Å, $\alpha = 78.732°$, $\beta = 83.014°$, and $\gamma = 81.832°$.

3.3. *Description of crystal structure*

An Oak Ridge Thermal Ellipsoid Plot (ORTEP) of the cationic part of **1** is shown in figure 1. Bond angle and distance parameters are tabulated in table 2. The structural description of $[Mn_3O_4(H_2O)_2(phen)_4](NO_3)_4 \cdot 3H_2O$ (**1**) is described elsewhere [12a]. The compound contains a triangle where Mn(IV) atoms are at vertices. Charge consideration, bond distance data [12], and Bond Valence Sum calculation confirm the oxidation state of each Mn in the molecule [13, 14]. Mn(1) is linked with the Mn(2) and Mn(3) with a single oxo bridge, and Mn(2) and Mn(3) are linked with a double oxo bridge. Each Mn is in distorted octahedral environment. From bond angle and bond distance values, for Mn(1), O(6) [oxo O], and N(7) [imine N] are in axial positions, and N(5), N(6), N(8) [each imine N], and O(9) [oxo O] are in equatorial positions. For Mn(2), O(4) [oxo O] and O(1w) [O from water] are axial and N(1), N(2) [imine N], O(3), O(6) [oxo O] are equatorial. For Mn(3), O(3), and O(2w) are axial, and N(9), N(10) [imine N], O(4), O(9) [oxo O] are equatorial. In solid-state **1** forms a 3-D structure (figure 2) through C–H$\cdots\pi$ and $\pi\cdots\pi$ interactions (table 3).

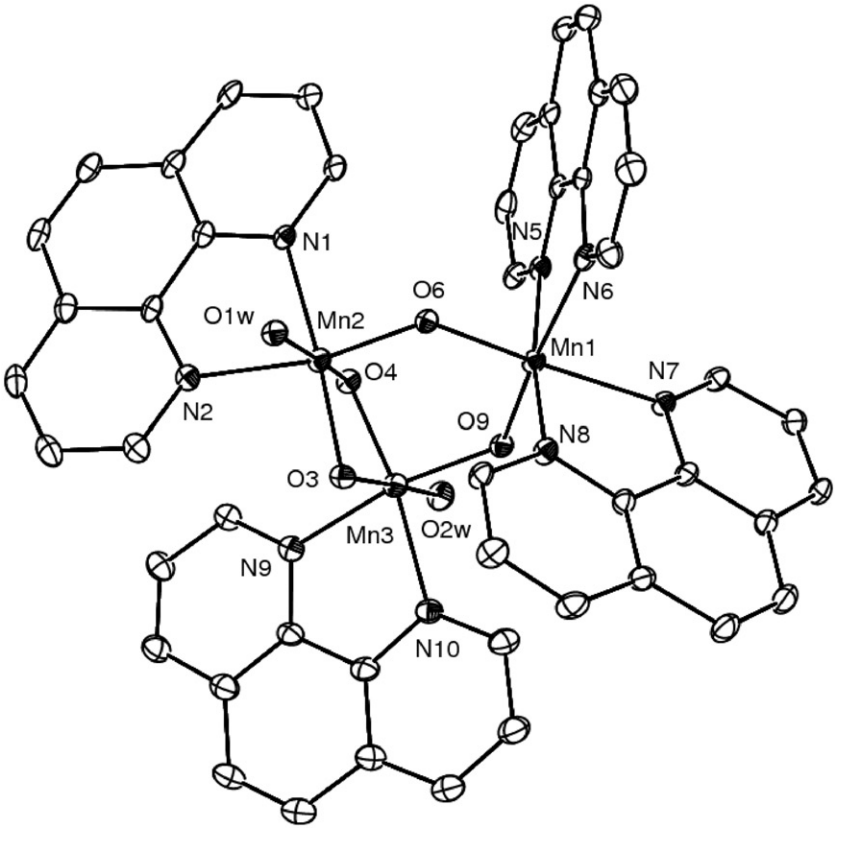

Figure 1. ORTEP diagram of $[Mn_3(phen)_4(O)_4(OH_2)_2]^{4+}$.

Table 2. Bond distance and angle data of $[Mn_3(phen)_4(O)_4(OH_2)_2](NO)_4 \cdot 3H_2O$.

Mn(1)–O(6)	1.774(5)	Mn(2)–O(1w)	1.991(5)
Mn (1)–O(9)	1.761(5)	Mn(2)–N(1)	2.063(6)
Mn (1)–N(5)	2.016(8)	Mn(2)–O(3)	2.060(6)
Mn(1)–N(6)	2.072(8)	Mn(3)–O(3)	1.793(5)
Mn (1)–N(7)	2.098(7)	Mn(3)–O(4)	1.790(4)
Mn(1)–N(8)	2.002(7)	Mn(3)–O(9)	1.816(5)
Mn(2)–O(3)	1.799(4)	Mn(3)–O(2w)	1.997(6)
Mn(2)–O(4)	1.790(5)	Mn(3)–N(9)	2.049(8)
Mn(2)–O(6)	1.815(5)	Mn(3)–N(10)	2.057(6)
O(6)–Mn(1)–O(9)	99.3(2)	O(6)–Mn(2)–N(1)	92.0(2)
O(6)–Mn(1)–N(5)	89.0(3)	O(6)–Mn(2)–N(2)	165.4(3)
O(6)–Mn(1)–N(6)	85.8(2)	O(8)–Mn(2)–N(1)	91.3(2)
O(6)–Mn(1)–N(7)	173.0(3)	O(8)–Mn(2)–N(2)	83.1(2)
O(6)–Mn(1)–N(8)	95.9(3)	N(1)–Mn(2)–N(2)	78.7(3)
O(9)–Mn(1)–N(5)	96.7(3)	O(3)–Mn(3)–O(4)	82.8(2)
O(9)–Mn(1)–N(6)	174.1(2)	O(3)–Mn(3)–O(2w)	176.2(2)
O(9)–Mn(1)–N(7)	86.8(3)	O(3)–Mn(3)–N(9)	89.8(2)
O(9)–Mn(1)–N(8)	90.6(2)	O(3)–Mn(3)–N(10)	89.9(2)
N(5)–Mn(1)–N(6)	80.3(3)	O(4)–Mn(3)–O(9)	95.7(2)
N(5)–Mn(1)–N(7)	93.8(3)	O(4)–Mn(3)–O(2w)	95.3(2)
N(5)–Mn(1)–N(8)	170.5(3)	O(4)–Mn(3)–N(9)	93.9(3)
N(6)–Mn(1)–N(7)	88.3(3)	O(4)–Mn(3)–N(10)	169.8(3)
N(6)–Mn(1)–N(8)	91.9(3)	O(9)–Mn(3)–O(2w)	85.5(2)
N(7)–Mn(1)–N(8)	80.4(3)	O(9)–Mn(3)–N(9)	168.4(2)
O(3)–Mn(2)–O(4)	82.6(2)	O(9)–Mn(3)–N(10)	92.5(3)
O(3)–Mn(2)–O(6)	95.9(2)	O(2w)–Mn(3)–N(9)	87.1(2)
O(3)–Mn(2)–O(1w)	98.95(19)	O(2w)–Mn(3)–N(10)	91.6(3)
O(3)–Mn(2)–N(1)	167.5(3)	N(9)–Mn(3)–N(10)	78.8(3)
O(3)–Mn(2)–N(2)	95.3(3)	O(3)–Mn(3)–O(9)	97.9(2)
O(4)–Mn(2)–O(6)	98.3(2)	Mn(2)–O(4)–Mn(3)	96.0(2)
O(4)–Mn(2)–O(1w)	175.4(2)	Mn(1)–O(6)–Mn(2)	129.4(3)
O(4)–Mn(2)–N(1)	86.6(2)	Mn(1)–O(9)–Mn(3)	130.0(3)
O(4)–Mn2–N(2)	92.4(2)	Mn(2)–O(3)–Mn(3)	95.6(2)
O(6)–Mn(2)–O(1w)	86.0(2)		

Table 3. C–H$\cdots\pi$ and $\pi\cdots\pi$ interactions (Å, °) for **1**.

X–H$\cdots$Cg	H$\cdots$Cg	X$\cdots$Cg	X–H$\cdots$Cg (°)
C(59)–H(59)$\cdots$Cg(2)[a]	2.90	3.748(10)	153
C(59)–H(59)$\cdots$Cg(10)	2.75	3.336(9)	122
C(59)–H(59)$\cdots$Cg(18)	2.96	3.817(10)	155
C(45)–H(45)$\cdots$Cg(3)	2.86	3.679(11)	148
C(45)–H(45)$\cdots$Cg(19)	2.99	3.785(12)	144
C(42)–H(42)$\cdots$Cg(3)	2.97	3.258(10)	100
$\pi\cdots\pi$ Interactions (Å, °)			
Cg–Cg	Cg–Cg distance	Dihedral angle (i,j)	Perpendicular distances between baricentres (i,j)
Cg8$\cdots$Cg8[b]	3.398(5)	0	3.334(3)

Symmetry codes: [a]x, y, z; [b]x, $1-y$, $1-z$.

3.4. *Magnetism*

The magnetic properties of **1** were investigated from 1.8 to 300 K. A plot of $\chi_M T$ *versus* temperature is shown in figure 3, where χ_M is the molar magnetic susceptibility. At

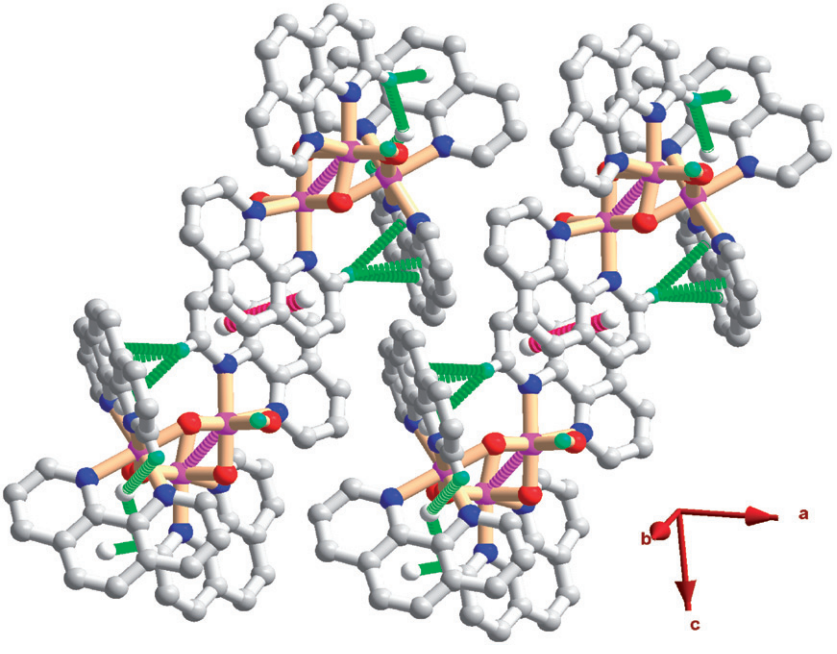

Figure 2. 3-D structure of **1** in the solid-state through C–H$\cdots\pi$ and $\pi\cdots\pi$ interactions.

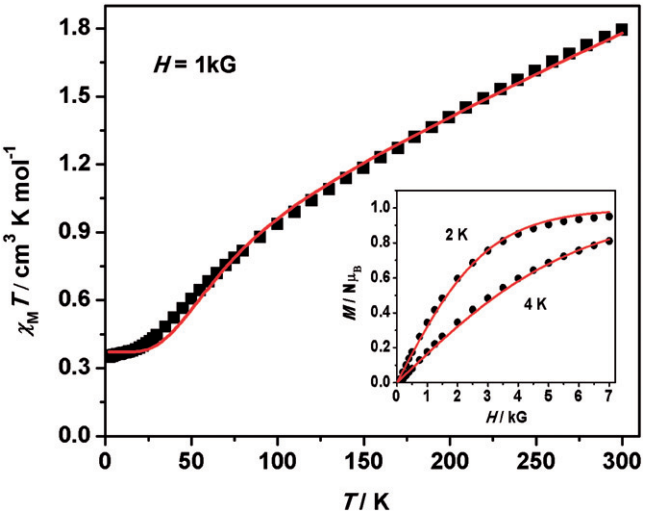

Figure 3. Temperature dependence of $\chi_M T$ for **1** at applied magnetic field of 1 kG. Inset: Field dependence of the magnetization for **1** at 2 and 4 K. The solid lines represent calculated curves with the parameters given in the text.

room temperature $\chi_M T$ is 1.79 $cm^3 K mol^{-1}$ and decreases rapidly on cooling to reach 0.35 $cm^3 K mol^{-1}$ at 2 K, indicative of strong antiferromagnetic coupling between metal ions. Data were analyzed with MAGPACK [15] using the spin-Hamiltonian described

in equation (1), where J_1 describes the interaction across the two mono-μ-oxo bridges in **1** and J_2 is the exchange coupling across the di-μ-oxo bridge.

$$H = -2J_1(S_1S_2 + S_1S_3) - 2J_2S_2S_3 \quad (1)$$

Both susceptibility *versus* temperature and magnetization versus field data were well modeled with the following set of parameters: $g = 1.99$, $J_1 = -50.0\,\mathrm{cm}^{-1}$, and $J_2 = -90.2\,\mathrm{cm}^{-1}$. Calculation of the spin state energies indicates that **1** has an S = ½ ground state, with an S = 3/2 excited state at *ca* $95\,\mathrm{cm}^{-1}$. These values compare well with those reported for related systems featuring a triangular $[Mn_3^{IV}O_4]$ core [6a].

3.5. *X-ray photoelectron spectroscopy*

The Mn 2p core level spectrum of **1** is given in figure 4. The characteristic peak indicates that each Mn is in 4+ valence state. The binding energy of Mn 2p3/2 peak at 643 eV is higher compared to that of Mn in MnO_2. This may be explained in the fact that the Mn ion in the present compound is in a more electronegative environment than MnO_2.

3.6. *Thermal study*

The thermal behavior of **1** was followed to 900°C under nitrogen with a heating rate of 10°C per minute. Compound **1** decomposes in three steps (Supplementary material). The first step between 4°C and 129°C corresponds to an endothermic process with loss of three crystal waters with mass loss of 4.742% (Calcd 4.197%). Release of four nitrates takes place in the second step (129–267°C). The experimental mass loss of 16.056% agrees with the calculated loss of 19.261%. In the third step, the coordination

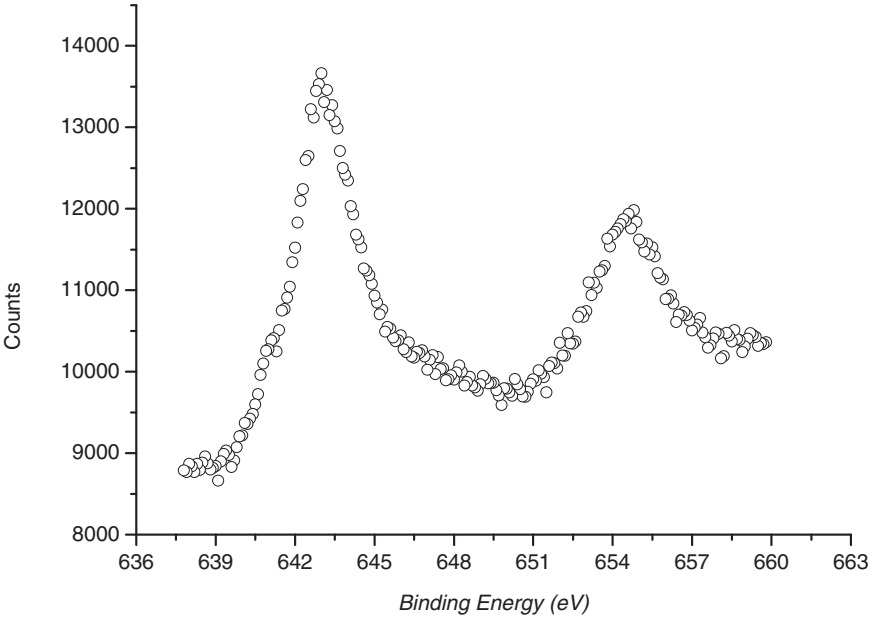

Figure 4. Mn2p core level X-ray photoelectron spectrum of **1**.

environment of the trinuclear manganese compound is broken between 267°C and 553°C. Loss of four phenanthrolines with two coordinated waters occurred. The experimental mass loss of 58.4% agrees with the calculated mass loss of 59.1%. After 900°C the residual ash of **1** is collected and its IR spectrum recorded. The IR spectrum of the residual ash is identical to MnO_2 (Supplementary material).

4. Conclusions

We have elaborated the synthesis and crystal structure of a trinuclear manganese (IV) compound which shows strong antiferromagnetic coupling between metal centres. The compound has an $S = ½$ spin ground state, with an $S = 3/2$ excited state at *ca* 95 cm^{-1}. Similar homovalent manganese trinuclear species reveals that +IV, +II valencies at each manganese generates strong antiferromagnetic behavior [12a, 16], whereas +III oxidation states gives high spin ground states as Jahn-Teller active nearly octahedral Mn(III) complexes have single-ion anisotropy [3d]. Stepwise degradation of **1** and final conversion to MnO_2 have been found when heated from room temperature to 900°C. The magnetic and thermal properties of the compound are an addition to manganese cluster chemistry.

Supplementary material

CCDC 757 110 (**1**) contains the supplementary crystallographic data for **1**. These data can be obtained free of charge *via* http://www.ccdc.cam.ac.uk/conts/retrieving.html or from the Cambridge Crystallographic Data Centre, 12 Union Road, Cambridge CB2 1EZ, UK; Fax: (+44) 1223-336-033; or E-mail: deposit@ccdc.cam.ac.uk

Acknowledgments

Financial support by the Department of Science & Technology (DST), New Delhi, India (No. SR/FT/CS-83/2010 dt. 11-02-2011) is gratefully acknowledged by RG. Authors sincerely thank Dr Pabitra K. Chakrabarti, Department of Physics, The University of Burdwan, Burdwan 713 104, India and Dr Md. Motin Seikh, Department of Chemistry, Visva-Bharati, Shantiniketan 731 235, India for PXRD data collection and their analysis. Single crystal X-ray crystallography was performed at the DST funded National Single Crystal X-ray diffraction facility at the Department of Inorganic Chemistry, IACS, Kolkata.

References

[1] (a) O. Kahn, *Molecular Magnetism*, VCH Publishers, New York (1993); (b) J.S. Miller, M. Drillon (Eds.), *Magnetism: Molecules to Materials IV*, Wiley, Weinheim (2003); (c) M. Verdaguer. *Polyhedron*, **20**, 1115 (2001).

[2] (a) I. Bertini, H.B. Gray, S.J. Lippard, J.S. Valentine. *Bioinorganic Chemistry*, Viva Books Pvt. Ltd., India (1998); (b) J. Raymond, R.E. Blankenship. *Coord. Chem. Rev.*, **252**, 377 (2008); (c) J. Barber. *Inorg. Chem.*, **47**, 1700 (2008). (d) A.K. Dutta, R. Ghosh. *Inorg. Chem. Commun.*, **14**, 337 (2011).
[3] (a) G. Christou, D. Gatteschi, D.N. Hendrickson, R. Sessoli. *MRS. Bull.*, **25**, 66 (2000); (b) G. Aromi, E.K. Brechin. *Struct. Bond.*, **122**, 1 (2006); (c) D. Gatteschi, R. Sessoli. *Angew. Chem. Int. Ed.*, **42**, 268 (2003); (d) T.C. Stamatatos, D. Foguet-Albiol, C.C. Stoumpos, C.P. Raptopoulou, A. Terzis, W. Wernsdorfer, S.P. Perlepes, G. Christou. *Polyhedron*, **26**, 2165 (2007).
[4] J.R. Friedman, M.P. Sarachik, J. Tejada, R. Ziolo. *Phys. Rev. Lett.*, **76**, 3830 (1996).
[5] W. Wernsdorfer, R. Sessoli. *Science*, **284**, 133 (1999).
[6] (a) N. Auger, J.J. Girerd, M. Corbella, A. Gleizes, J.L. Zimmermann. *J. Am. Chem. Soc.*, **112**, 448 (1990); (b) R. Ramaraj, A. Kira, M. Kaneko. *Angew. Chem. Int. Ed. Engl.*, **25**, 825 (1986).
[7] D.P. Kessissoglou. *Coord. Chem. Rev.*, **837**, 185 (1999).
[8] SHELXTL 5.10, Bruker Analytical X-ray Instruments Inc., Karlsruche, Germany (1997).
[9] L.J. Farrugia. *ORTEP-32* for Windows, University of Glasgow, Scotland (1998).
[10] (a) K. Nakamoto, *Infrared and Raman Spectra of Inorganic and Coordination Compounds; Part B: Applications in Coordination, Organometallic, and Bioinorganic Chemistry*, John Wiley & Sons Inc., New York (1997); (b) S. Barbara, *Infrared Spectroscopy: Fundamentals and Applications*, Wiley, New York (2004).
[11] J. Rodriguez-Carvajal. *An Introduction to the Program FULLPROF 2000*, Laboratoire Léon Brillouin, CEA-CNRS: Saclay, France (2001).
[12] (a) K.R. Reddy, M.V. Rajasekharan, N. Arulsamy, D.J. Hodgson. *Inorg. Chem.*, **35**, 2283 (1996); (b) M. Murugesu, W. Wernsdorfer, K.A. Abboud, G. Christou. *Polyhedron*, **24**, 2894 (2005); (c) M. Soler, E. Rumberger, K. Folting, D.N. Hendrickson, G. Christou. *Polyhedron*, **20**, 1365 (2001).
[13] (a) P.L. Roulhac, G.J. Palenik. *Inorg. Chem.*, **42**, 118 (2003); (b) T. Taguchi, M.S. Thompson, K.A. Abboud, G. Christou. *Dalton Trans.*, **39**, 9131 (2010).
[14] Bond Valence Sum (BVS), an empirical quantity, has been used to determine the oxidation state of each Mn in **1** in solids from the crystallographically determined bond distance data. Bond valence $(S) = \exp.[(R_0 - R_{ij})/B]$, Oxidation state = Σ bond valences; R_{ij} is the observed bond length, the usual procedure is to assume an oxidation state and to use previously determined R_0 values appropriate to the bond being considered. The constant B is determined as 0.37. If in the present complex Mn is assumed to have +IV oxidation state then R_0 for Mn–O and Mn–N are 1.753 and 1.825 Å, respectively. (i) Now for Mn1, Σ bond valences = (0.9707 + 0.9422) [for Mn–O bonds] + (0.6164 + 0.5887 + 0.6114 + 0.4755) [for Mn–N bonds] = 4.2049; so oxidation state of Mn1 is + IV. (ii) For Mn2, Σ bond valences = (0.9048 + 0.8688 + 0.8503 + 0.5370) [for Mn–O bonds] + (0.5270 + 0.5171) [for Mn–N bonds] = 4.205; so oxidation state of Mn2 is +IV. (iii) For Mn2, Σ bond valences = (0.8902 + 0.8830 + 0.8411 + 0.5227) [for Mn–O bonds] + (0.5429 + 0.5270) [for Mn–N bonds] = 4.206; so oxidation state of Mn3 is +IV.
[15] J.J. Borras-Almenar, J.M. Clemente-Juan, E. Coronado, B.S. Tsukerblat. *J. Comput. Chem.*, **22**, 985 (2001).
[16] (a) N. Auger, J.-J. Girerd. *J. Am. Chem. Soc.*, **112**, 448 (1990); (b) D. Tian, Y. Pang, S. Guo, X. Zhu, H. Zhang. *J. Coord. Chem.*, **64**, 1006 (2011).